THE JOURNAL OF PHYSICAL CHEMISTRY C
A JOURNAL OF THE AMERICAN CHEMICAL SOCIETY

pubs.acs.org/JPCC

Article

Depletion-Driven Assembly of Polymer-Coated Nanocrystals

Allison M. Green, Sanket Kadulkar, Zachary M. Sherman, Thomas M. Fitzsimons, Charles K. Ofosu, Jiajun Yan, David Zhao, Jan Ilavsky, Adrianne M. Rosales, Brett A. Helms, Venkat Ganesan, Thomas M. Truskett,* and Delia J. Milliron*

Cite This: J. Phys. Chem. C 2022, 126, 19507−19518

Read Online

ACCESS | Metrics & More | Article Recommendations | Supporting Information

ABSTRACT: Depletion-driven assembly has been widely studied for micrometer-sized colloids, but questions remain at the nanoscale where the governing physics are impacted by the stabilizing surface ligands or wrapping polymers, whose length scales are on the same order as those of the colloidal core and the depletant. Here, we probe how wrapping colloidal tin-doped indium oxide nanocrystals with polymers affects their depletion-induced interactions and assembly in solutions of poly(ethylene glycol). Copolymers of poly(acrylic acid) grafted with poly(ethylene oxide) provide nanocrystal wrappings with different effective polymer graft densities and molecular weights. (Ultra)-small-angle X-ray scattering, coarse-grained molecular dynamics simulation, and molecular thermodynamic theory were combined to analyze how depletant size and polymer wrapping characteristics affect depletion interactions, structure, and phase behavior. The results show how depletant molecular weight, as well as surface density and molecular weight of polymer grafts, sets thresholds for assembly. These signatures are unique to depletion-driven assembly of nanoscale colloids and mirror phase behaviors of grafted nanoparticle−polymer composites. Optical and rheological responses of depletion-driven assemblies of nanocrystals with different polymer shell architectures were probed to learn how their structural differences impact properties. We discuss how these handles for depletion-driven assembly at the nanoscale may provide fresh opportunities for designing responsive depletion interactions and dynamically reconfigurable materials.

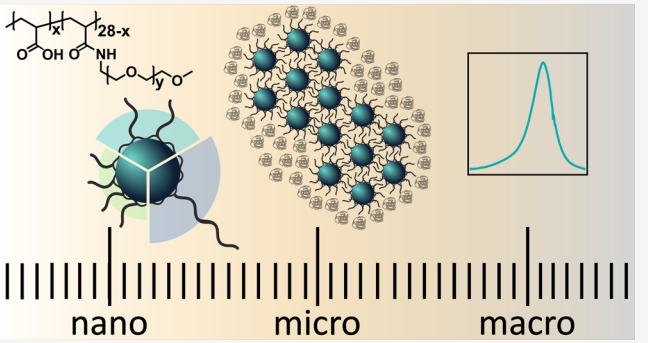

INTRODUCTION

Colloidal nanocrystals (NCs) exhibit size- and composition-dependent optical and electronic properties[1,2] which make them attractive material building blocks for applications from optoelectronics to catalysis. Through assembly, NC-based materials acquire emergent properties as evidenced by, for example, shifts in optical absorption of tin-doped indium oxide (ITO) NCs upon gelation.[3−5] The spatial arrangement, i.e., structure, of nanoparticles in hybrid materials can significantly impact ion or proton conductivity[6−9] and mechanical properties.[10−13] Developing strategies to systematically tune the interactions that influence nanoparticle structure and structure-dependent properties of functional nanomaterials is essential for their design.

NC surfaces are commonly capped with ligands to ensure colloidal stability or to add functionality.[14] As an alternative to hydrocarbon ligands or end-functionalized polymers, random copolymers may be employed to wrap NC surfaces.[15] This polymer-wrapping approach has been commonly used to leverage polymer characteristics (e.g., chirality, size, and dispersibility) to assist in the purification of carbon nanotubes.[16,17] Though copolymers add complexity, they also provide an opportunity to influence interactions and properties. For example, one can synthetically modify the composition or structure of polymer components to achieve more than one aim, e.g., binding to the NC surface and mediating the interaction with the environment.[18] For the case of copolymer-grafted particles, macromolecular design has been leveraged to optimize thermoresponsive behavior for drug delivery,[19] to tailor mechanical robustness in composites,[20] and to modify ion content and conductivity in membranes.[21] Likewise, polymer wrapping has been used to direct nanoparticle surface charge,[22] to compatibilize NCs with cell culture medium,[23,24] and to prepare mechanically robust hydrogel composites.[25] By tuning the arrangement of nanoparticles and thereby their properties as well, assembly provides another degree of control over material design and functionality.

Received: September 1, 2022
Revised: October 19, 2022
Published: November 7, 2022

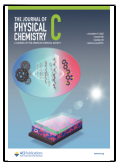

Chemical methods for displacing or linking to surface ligands have been widely employed to direct NC assembly.[4,26−31] However, such approaches intrinsically limit the composition or chemistry of the surface ligands to those appropriate for the chosen aggregation mechanism. Depletion interactions, entropic effective attractions between colloids mediated by addition of *nonadsorbing* macromolecular depletants, offer an alternative approach for promoting NC assembly. In the latter case, the effective interaction range and strength depend on the depletant and colloid sizes as well as the depletant concentration.[32−34] Because of its nonspecific nature, the depletion mechanism has been applied to assemble both nanoscale[35−37] and micrometer-sized[38−40] colloids with different shapes and compositions.

Depletion attractions between microparticles and their implications for phase behavior are well understood.[32,41−43] Even when large geometric variations (compared to depletant size) are present at the surfaces of micrometer-scale colloids, e.g., due to concavity[44] or roughness,[45−47] the implications for depletion interactions can be quantitatively predicted based on how they change the overlap of depletant exclusion volumes of neighboring particles. Similar concepts have been extended to qualitatively understand depletion-driven assembly of nanoparticles[48−53] and proteins[54−62] with the aid of theoretical predictions.[63−69] However, compared to micrometer-sized colloids, depletion interactions at the nanoscale are more nuanced and challenging to quantify as the characteristic size of the colloid becomes comparable to those of surface heterogeneities, ligands, and even solvent molecules.[61,70]

Although depletion interactions have been successfully applied to direct NC assembly,[37] predicting phase behavior and structure remains challenging in part because little is known about how the composition and molecular structure of capping ligands or wrapping polymers mediate the depletion interactions between NCs. Here, we study these questions using colloidal ITO NCs that are surface wrapped with copolymers of poly(acrylic acid) and poly(ethylene oxide) (PEO). Depletion attractions are induced by adding poly(ethylene glycol) (PEG) of varying molecular weights (*MW*s) and concentrations. Using X-ray scattering and coarse-grained molecular dynamics (MD) simulations, we analyze the resulting microstructures, and we interpret the phase behavior using a molecular thermodynamic model. We find that depletion attractions are effective for driving assembly of polymer-wrapped NCs. Moreover, through variations in the PEO surface polymer graft density and *MW*, we demonstrate that the polymer shell structure significantly modifies the depletion attraction—in ways analogous to behavior of grafted nanoparticle−polymer composites[68,71,72]—with implications for phase behavior, rheology, and optical properties. Perhaps the most striking consequence is the emergence of a depletant *MW* threshold for assembly that depends on the architecture of the polymer wrapping. This behavior, which is specific to depletion interactions at the nanoscale, helps to explain why strong, short-range attractions (and gelation as an assembly outcome) are avoided in these materials.[41] On the basis of our analysis, we suggest mechanistic interpretations of these results and promising directions for future research.

■ EXPERIMENTAL SECTION

Following established methods, ITO NCs were synthesized via the slow injection of metal precursor In(III) acetate, Sn(IV) acetate, and oleic acid) into oleyl alcohol.[73] After the reaction was cooled from 290 °C, the NCs were purified by centrifuging with isopropanol as the antisolvent and redispersing in hexane three times. Subsequently, the NCs were stripped of their native, hydrophobic ligands (oleate). Nitrosonium tetrafluoroborate ($NOBF_4$) was used to remove the ligands and transfer the NCs to dimethylformamide.[74] The resulting NC dispersion was then washed seven times via centrifugation with toluene as the antisolvent and redispersed in dimethylformamide.

The NCs were wrapped with a graft copolymer of poly(acrylic acid) and poly(ethylene oxide) monomethyl ether (PAA−*m*PEO). Variations of the copolymer were synthesized via a previously reported method to maintain the same length backbone while tuning the number of acrylic acid monomers and the length and number of PEO grafts.[75] A previous polymer wrapping procedure was adapted.[15,76] The ligand-stripped NCs were centrifuged and redispersed in acetonitrile (ACN). Separately, PAA−*m*PEO was dissolved in ACN. The NC dispersion in ACN was added dropwise to the polymer solution while stirring at 400 rpm. The solution was stirred for 24 h to wrap the NC surfaces. To remove excess polymer, ultrafiltration was performed three times. Following purification, the dispersion was further concentrated via solvent evaporation to the desired NC volume fraction.

Various molecular weights (5, 10, 20, and 35 kDa) and concentrations of PEG were then added to the concentrated NC dispersions via sonication to study assembly via depletion attractions. The microstructure of the resulting colloidal systems were analyzed via ultra-small and small-angle X-ray scattering (USAXS and SAXS). A SAXSLAB GANESHA was used for SAXS transmission measurements on flame-sealed capillary samples. Additional samples were sent to Argonne National Laboratory Advanced Photon Source beamline 9ID for USAXS/SAXS measurements.[77]

Bright-field scanning transmission electron microscopy (STEM) was performed on dilute samples dropcast on carbon support films on copper grids using a Hitachi S5500 microscope. Nuclear magnetic resonance (NMR) ^{1}H spectra were collected on a MR400 system, with samples prepared in D_2O. Thermogravimetric analysis (TGA) was conducted on samples in alumina crucibles with a Mettler Toledo TGA 2. Samples were dried overnight under vacuum prior to measurement. Dynamic light scattering (DLS) and zeta-potential (ZP) measurements were performed using a Zetasizer Nano ZS on dilute samples (2 mg/mL) in glass cuvettes (with a dip cell for ZP). Fourier-transform infrared (FTIR) spectroscopy was performed on samples in a liquid cell with potassium bromide windows (hexane) or calcium fluoride windows (acetonitrile) using a Bruker VERTEX 70 FTIR. Rheometry experiments were performed using a 20 mm diameter 2° stainless steel cone geometry with a solvent trap on a TA Instruments Discovery HR2 rheometer. Samples filled the geometry gap, and the solvent trap was filled with acetonitrile to prevent solvent evaporation from the sample.

Molecular Dynamics (MD) Simulation Methods. We performed molecular simulations to help understand the depletion interactions underlying the structural characteristics observed experimentally. Simulations of detailed atomistic models including NCs with surface-wrapped polymers and polymeric depletants would be computationally intractable. We instead employed MD simulations of coarse-grained models to compute the potential of mean force (PMF) between two surface-functionalized NCs dispersed in a matrix representing a concentrated solution of polymer depletants. The effective

https://doi.org/10.1021/acs.jpcc.2c06279
J. Phys. Chem. C 2022, 126, 19507−19518

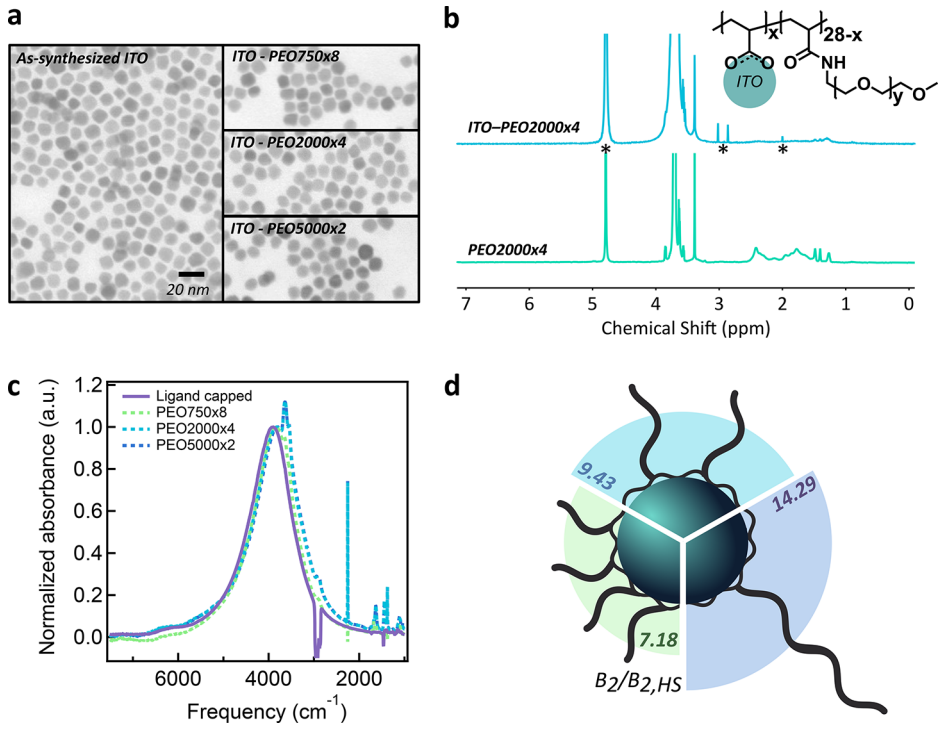

Figure 1. (a) Bright-field STEM images of NCs before and after wrapping with each surface polymer. (b) ^{1}H NMR spectra of free polymer (bottom) and the corresponding polymer-wrapped NCs (top). Stars (∗) below the NC spectrum indicate solvent peaks (H_2O, dimethylformamide, ACN). Inset: schematic of copolymer binding to NC. (c) NC LSPR spectra before and after wrapping with each surface polymer. (d) Schematic of polymer-wrapped NCs with relative grafting length and densities (green, PEO750x8; turquoise, PEO2000x4; blue, PEO5000x2), giving rise to increasing repulsion evidenced by second virial coefficient measurement. Each shaded sector plus core is proportional to the NC effective hard sphere radius calculated from B_2 (10.9, 12.0, and 13.7 nm, respectively).

NC−NC interactions were computed for different design points by varying the surface polymer graft *MW* and density and the *MW* of the depletant.

The coarse-grained model was adapted from a previous simulation study.[78] To compute PMF, we use an orthogonal simulation cell with an aspect ratio of 2:1:1 and triply periodic boundary conditions. The NCs are fixed at positions $(-r/2,0,0)$ and $(r/2,0,0)$ for a series of separation distances r. The volume fraction occupied by the NCs was fixed to be 0.0238. A PAA−*m*PEO copolymer was used to wrap the NCs, with the PAA groups wrapping the NC surface, while the PEO grafts extend out from the surface.[15] Given this copolymer architecture, we adopt a coarse-grained model that represents the polymer shell as end-grafted PEO chains. The surface of each NC was grafted with N_g polymers each consisting of L_g beads. The size of each bead was considered a Kuhn length for PEO (i.e., $1\sigma \approx 7.6$ Å).[79] Accordingly, on the basis of the size of the NC core (determined by SAXS of a dilute dispersion), each NC core was modeled as a sphere with radius 7.5σ. N_g was assigned to be the corresponding average number of PEO grafts per NC obtained by multiplying the experimental copolymer wrapping density from TGA by the number of PEO grafts per copolymer. The numbers of beads in each chain of the graft (L_g) and the depletant (L_m) were decided based on the *MW* of the PEO side chain in the copolymer and the *MW* of PEG depletant, respectively. The total number of beads in the grafted chains and depletant polymers was fixed to be 126000, corresponding to a bead density of $0.85\sigma^{-3}$. The details pertaining to the simulation model, methodology, and the PMF calculations are presented in the Supporting Information.

Phase Diagram Calculations. We model the phase behavior of a mixture of polymer wrapped nanocrystals and nonadsorbing polymer depletant using generalized free volume theory, an extension of free volume theory for interacting polymer depletants in the semidilute regime.[32] We incorporate Yukawa repulsions into generalized free volume theory following the procedure from ref 80. NCs were modeled as hard spheres of radius a_{HS} that interacted with other NCs via hard-sphere repulsions and soft pairwise Yukawa repulsions. The soft repulsions are parametrized by a contact strength ε_Y and range λ_Y. Depletant polymers were modeled as excluded volume chains in a good solvent of known radius of gyration R_g with an osmotic pressure obtained from renormalization group theory.

The core radius of the NCs is a_{core} = 5.82 nm (SAXS form factor fitting), but because of the polymer wrapping, the effective hard core (a_{HS}) that the polymer depletant interacts with is larger ($a_{HS} \geq a_{core}$). We treat a_{HS} and λ_Y as fit parameters, with ε_Y chosen such that the virial coefficient with no depletant equals the experimentally measured virial coefficient B_2/B_{HS} = 9.43. For each a_{HS}, we compute the fluid/fluid binodal for a series of λ_Y values. We then select the λ_Y value for the fluid/fluid binodal that is closest to the experimentally observed assembly boundary in a least-squares sense. We find a curve of (a_{HS}, λ_Y) pairs with binodals consistent with the experimental data. We select one a_{HS} whose λ_Y value is consistent with two NC polymer layers each of thickness $\approx 2R_g$. The result of this fitting procedure is a_{HS} = 8.00 nm, λ_Y = 4.88 nm, and $\varepsilon_Y = 3.62\ k_BT$.

https://doi.org/10.1021/acs.jpcc.2c06279
J. Phys. Chem. C 2022, 126, 19507−19518

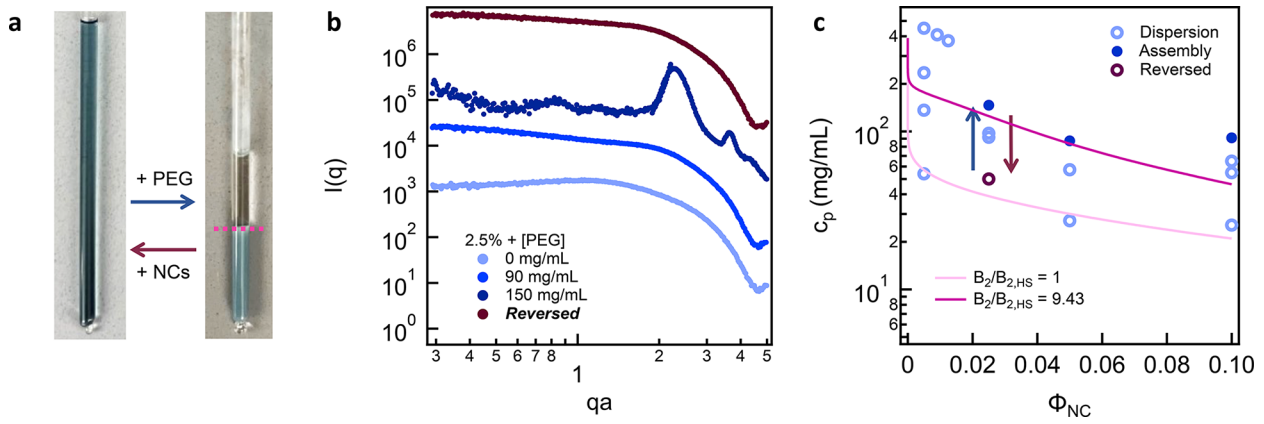

Figure 2. (a) Photographs of (left) a NC dispersion and (right) phase-separated NC assembly in capillaries. (b) SAXS intensities as a function of the wave vector q nondimensionalized by the NC core radius from SAXS form factor fitting a for 2.5% v/v polymer-wrapped NCs (PEO2000x4) with varying concentration of 20 kDa PEG depletant added, offset for clarity. (c) Experimental phase diagram (depletant concentration vs NC volume fraction) overlaid on theoretical calculated fluid-fluid binodals for hard spheres (light line) and adjusted to add short-ranged surface repulsion (dark line).

RESULTS AND DISCUSSION

Nanocrystal Polymer Wrapping. Wrapping the NC surface with a copolymer is a versatile approach because the polymer is bifunctional. One component is selected for its propensity to bind the NC surface while the other can be independently selected to introduce a new property to the system, e.g., enhanced solubility. Here, PAA−*m*PEO was chosen to wrap ITO NCs because PAA carboxylic acid groups readily bind to the metal oxide surface, while PEO brushes confer dispersibility in ACN. PEG depletants, which introduce attractions to drive assembly, are also highly soluble in ACN and expected to be nonadsorbing on the PEO grafts.

ITO NCs were synthesized via a slow injection method. Their native ligands were removed via $NOBF_4$ ligand stripping, and their bare surfaces were then wrapped with PAA−*m*PEO copolymers in ACN. The copolymers consist of varying ratios of PAA and PEO, the latter incorporated as a side-chain graft. Their chemical formulas are as follows: PAA_{26}-*g*-$(PEO5000)_2$, PAA_{24}-*g*-$(PEO2000)_4$, and PAA_{20}-*g*-$(PEO750)_8$ (Figures S1−S3). PAA-based polymer coatings provide a general platform for passivating NC surfaces where PAA coordinates to surface sites while a functional end-group or copolymer (PEO in this case) extends from the surface.[15] The principal difference between these wrapping polymers is the length and number of PEO side chains. They are termed PEO5000x2, PEO2000x4, and PEO750x8, respectively. STEM images of the NCs before and after polymer wrapping show no significant change in particle morphology (Figure 1a). The broadening of NMR peaks corresponding to the copolymer for polymer-wrapped NCs as compared to the free polymer spectra indicates that the polymer is successfully bound to the NC surface (Figures 1b and S4).[81] To further confirm successful polymer wrapping, FTIR spectra of dilute NC dispersions were taken before and after wrapping. The line shape and frequency of the strong absorption peak due to localized surface plasmon resonance (LSPR) of the NCs are nearly unaffected by the ligand stripping and wrapping procedure, with no signs of aggregation-induced LSPR coupling (Figure 1c). Note the sharp peaks in the spectra are due to vibrational modes of the surface polymers (Figures S5−S8).

TGA of each polymer-wrapped NC dispersion indicates an equivalent number loading on the NC surface (0.18 polymer molecules nm^{-2}) (Figure S9), demonstrating that the wrapping density is independent of copolymer composition. However, because the number of PEO grafts varies on each copolymer, the effective PEO graft densities vary and are as follows: 1.56 nm^{-2} (PEO750x8), 0.75 nm^{-2} (PEO2000x4), and 0.34 nm^{-2} (PEO5000x2). DLS and ZP measurements were conducted to further characterize the colloids after polymer wrapping. The distribution of diameters determined by DLS supports that we retain discrete NCs, whose hydrodynamic size increases with increasing length of PEO grafts on the surface polymer (Figure S10 and Table S1). A ZP measurement of 0 mV confirms the wrapped NCs surfaces have negligible charge (Figure S11).

All the polymer-wrapped NCs were indefinitely stable in ACN, but because the length and number of the PEO grafts trend inversely as polymer composition changes, their relative repulsive stabilization was not obvious *a priori*. To quantitatively determine the stabilizing repulsions due to polymer wrapping, the osmotic second virial coefficient (B_2) for each set of polymer-wrapped NCs divided by the hard-sphere virial coefficient corresponding to the NC core ($B_{2,expt}/B_{2,HS}$) was estimated via analysis of SAXS structure factors at varying NC concentration (Figures 1d and S12).[82,83] The experimental B_2 increases as the PEO graft *MW* increases, despite the correspondingly lower effective PEO graft density, indicating additional strength of repulsion and a larger effective NC size. Thus, the repulsive forces stabilizing the NCs against assembly are tunable via the copolymer structure and composition.

Depletion-Induced Assembly Phase Diagram. The experimental depletion phase diagram was probed by varying the concentration of 20 kDa PEG depletant added to PEO2000x4 NC dispersions at a series of NC core volume fractions (ϕ_{NC} = 0.025, 0.050, and 0.100). Upon dissolving incremental amounts of depletant, the threshold for assembly at each volume fraction was determined by visual inspection (cloudiness indicating assembly) (Figure S13 and Table S2). No visual changes were observed for samples below ϕ_{NC} = 0.025, indicating no significant NC clustering or aggregation. For higher NC volume fraction samples, assemblies slowly phase separated from a single cloudy phase, leading to a light blue transparent top phase and a cloudy blue bottom phase, and then ultimately to a clear top phase and a denser, cloudy

https://doi.org/10.1021/acs.jpcc.2c06279
J. Phys. Chem. C 2022, 126, 19507−19518

bottom phase (Figure 2a). The bottom phase contains the polymer-wrapped NCs, which have assembled to form aggregates, induced by depletion attraction.

SAXS was used to assess the microstructures of the NCs under varying preparation conditions. The SAXS analysis, used to evaluate whether NCs remain well-dispersed or whether assembled structure has emerged, supports the validity of the visually determined assembly threshold (Figure 2b). When the NC−polymer mixture remains transparent, the scattering pattern is nearly the same as the dilute NC form factor (Figure S14), suggesting no significant change in morphology. In contrast, cloudy samples exhibit a degree of ordering indicating assembly: a sharp, primary peak emerges. The suppression of scattering intensity at slightly lower q values than this peak, a correlation hole, is typical for phase separating systems as correlations in the concentrated phase develop.[84,85] Phase boundaries were determined via visual inspection, and corroborated with SAXS, for each of several NC volume fractions and concentrations of PEG depletant (Figure 2c).

To evaluate whether the observed phase behavior was consistent with depletion-induced attraction, theoretical phase boundaries were calculated using a molecular thermodynamic model that combines generalized free volume and scaled particle theory for depletion attractions. The model is parametrized with an NC hard-sphere radius a_{HS} and an estimate for the depletant polymer radius of gyration from light scattering measurements.[86] If NCs are considered as hard spheres with a radius equal to the core radius ($B_2/B_{2,HS} = 1$), neglecting any effect of their polymer wrapping, the predicted threshold severely underestimates the amount of depletant needed for assembly (Figure 2c). In fact, attempting to account for polymer wrapping by simply increasing the hard sphere radius relative to the core radius also always underestimates the assembly boundary (Figure S15). To account for the *soft* repulsive interaction provided by the polymer wrapping, we augmented the hard-core radius by a short-range Yukawa potential. This repulsive contribution, $U_Y = 2a_{HS}\varepsilon_Y r^{-1} \exp[-(r - 2a_{HS})/\lambda_Y)]$, is parametrized by the contact potential ε_Y and the range λ_Y.[32] The predicted phase diagram of this model, with physically reasonable values for these parameters, is consistent with the experimental assembly phase boundary (Figure 2c). These results indicate the phase behavior is consistent with depletion-induced demixing of polymer-wrapped NCs, where the wrapping serves to increase the depletant concentration threshold for assembly.

The measured osmotic second virial coefficient ($B_{2,expt}/B_{2,HS} = 9.43$) adds a constraint in choosing parameters of the model consistent with the experimental results. For example, shorter range repulsions (smaller λ_Y) require significantly larger ε_Y to match the experimental virial coefficient. A contact Yukawa potential, effective Yukawa repulsion length, and an effective hard sphere radius were found that are consistent with both the experimental virial coefficient and the experimental assembly threshold (Figures 2c and S15−S17). The calculated λ_Y is 4.88 nm, which matches expectations based on the molecular dimensions of the polymer grafts. The contact potential, constrained to the experimental B_2, is 3.62 k_BT. Thus, the phase behavior is, in fact, consistent with depletion-induced assembly with additional repulsions due to polymer wrapping. The phase behavior is also qualitatively similar to that of polymer-coated nanoparticle composites. In those systems, for sufficiently high *MW* of matrix polymer (relative to surface graft), an analogous entropically driven attraction between nanoparticles induces phase separation.[11,66,68,71,72,87,88]

In principle, assembly via depletion attractions is reversible. To test this, an assembled system was prepared by adding depletant to NCs at $\phi_{NC} = 0.025$. Then, additional NCs at $\phi_{NC} = 0.025$ were added to reduce the depletant concentration while maintaining the same NC volume fraction, returning to conditions on the phase diagram below the assembly threshold (Figure 2c). Upon manual agitation of the vial for 1 min, the cloudy assembly visually became transparent (Video S1). The visible reversal also resulted in a reversal of the SAXS intensity pattern to closely resemble that of the initial NC dispersion (Figure 2b). Thus, the NC polymer wrapping helps retain discrete NCs upon aggregation, preventing irreversible fusion and enabling facile reversal of assembly. Overall, for NCs wrapped with PEO2000x4 copolymer, assembly and disassembly induced by the 20 kDa PEG depletant occur as expected based on scale-independent depletion principles, once the additional surface polymer-related repulsions are understood and accounted for in the model.

Influence of Depletant Molecular Weight. The radius of gyration of the 20 kDa *MW* depletant is approximately 20% larger than the NC core radius. Commonly, smaller depletants (relative to the core size) are adopted, inducing strong, short-range colloidal attractions[36,38,42] which make gelation a more likely assembly outcome than equilibrium phase separation.[41] To probe how range of attraction affects depletion assembly of polymer-wrapped NCs, high concentrations of PEG depletants of varying *MW*s (10, 20, and 35 kDa), within solubility limits (Table S3), were added to dispersions of the PEO2000x4-wrapped NCs ($\phi_{NC} = 0.025$). Both 20 and 35 kDa PEG produced phase-separated assemblies within an hour, with condensed-phase structure also emerging in the SAXS pattern (Figure 3a). In contrast, the 10 kDa PEG sample remained a transparent blue with nearly the same scattering pattern as the form factor, indicating discretely dispersed NCs. Experiments conducted using 5 kDa PEG depletant also did not result in NC aggregation (Figure S18). As observed in grafted nanoparticle−polymer composite studies, there is a threshold depletant to graft chain length ratio (P/N), below which the particles are well-dispersed.[68,71,89] Here, the threshold falls between $P/N = 5$ (10 kDa depletant) and $P/N = 10$ (20 kDa depletant).

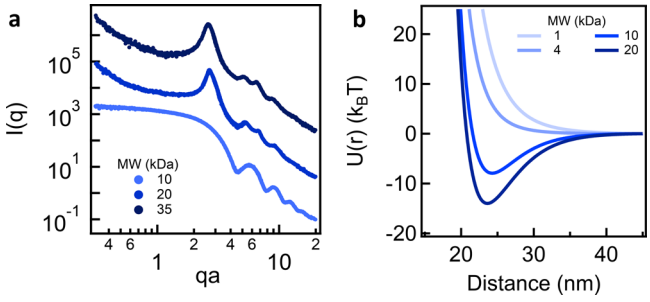

Figure 3. (a) SAXS intensities of 2.5% v/v polymer-wrapped NCs (PEO2000x4) with varying *MW* PEG depletants at high concentrations as shown in Table S2. Intensities arbitrarily offset for clarity. (b) Simulated PMF of NCs with polymer grafts modeled based on PEO2000x4 with varying *MW* PEG depletant.

Seeking to understand how depletant *MW* affects NC interactions, we performed coarse-grained MD simulations of

https://doi.org/10.1021/acs.jpcc.2c06279
J. Phys. Chem. C 2022, 126, 19507−19518

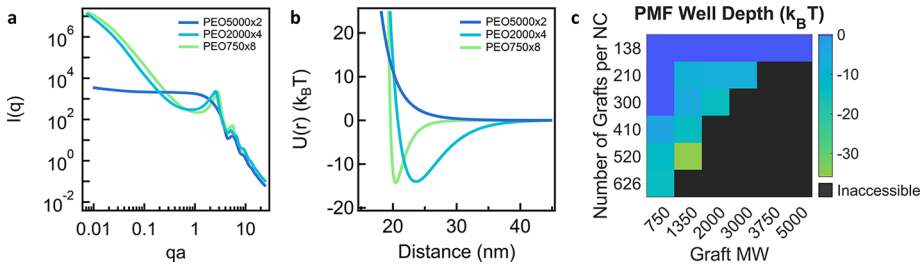

Figure 4. (a) USAXS/SAXS intensities for each polymer-wrapped NC upon addition of 35 kDa PEG depletant. (b) Simulated PMF for each copolymer wrapped NC in 20 kDa PEG depletant. (c) Simulated PMF attractive well depths for varying NC graft length and density in the presence of constant depletant *MW* (20 kDa).

two NCs with fixed grafting length and grafting density corresponding to that of the PEO2000x4 copolymer (Table S4). For concentrated depletant polymers with varied *MW* from 1 to 20 kDa, we calculated the PMF of the grafted NCs (Figure 3b). A threshold *MW* for the depletant is observed below which the PMF are purely repulsive. This result is consistent with the stable dispersions found experimentally for low-*MW* depletants (Figure 3a). With increasing depletant *MW* (increasing depletant-to-colloid size ratio), the simulated PMF crossover from purely repulsive to exhibiting longer-range attractive interactions; no *MW* depletant is consistent with the type of strong, short-range attractions that favor gelation. The predicted longer-range attractive interactions are consistent with the experimentally measured SAXS scattering intensities for the phase-separated systems with high-*MW* PEG depletants. Also consistent with these results, longer-range attractions between solvent-dispersed colloidal brushes were observed upon addition of nonadsorbing polymers of sufficient *MW* using Monte Carlo simulations[90,91] and density functional theory,[91] though in these earlier cases the attractions were weak due to the relatively low concentrations of added polymers.

This observation of a minimum depletant *MW* required to induce assembly contrasts with the behavior of other commonly studied depletion systems where assembly occurs, at sufficiently high depletant concentrations, for all depletant-to-colloid size ratios.[41,49,51] This highlights the distinctive role of the short-range repulsion near the NC surface added by the polymer wrapping, which should be overcome by the attractive depletant forces to induce assembly.[80,92] Considering the similar characteristic sizes of the components in our system, especially the polymer grafts and depletants, we wondered whether there are any more specific, structure-dependent effects of the polymer layer on depletion attractions and the resulting assemblies. As such, we endeavored to test, both experimentally and with simulations, the influence of the polymer graft length and density.

Copolymer Influence on Structure and Properties. To systematically investigate the impact of the polymer shell structure on the assembly of NCs via depletion attractions, depletant was added to NCs wrapped with copolymers of varying PEO graft *MW* and density (PEO750x8, PEO2000x4, and PEO5000x2). Upon addition of 35 kDa PEG depletant (300 mg/mL), the PEO750x8- and PEO2000x4-wrapped NCs became visually cloudy and phase separated into assemblies while the PEO5000x2-wrapped NCs remained transparent. Recall that as the PEO graft length increases, the $B_2/B_{2,HS}$ increases, indicating greater repulsions (Figure 1d). Therefore, the NCs with the largest magnitude of stabilizing repulsions are most resistant to depletant-induced assembly.

To evaluate how the properties of the grafted polymer influence the structure of the assemblies induced by depletion, USAXS/SAXS measurements were performed. The polymer shells are effectively invisible in these experiments due to their insignificant X-ray scattering contrast as compared to the inorganic NC cores, so the analysis is based upon the arrangement of cores. Consistent with the signatures of assembly and dispersion found when varying the *MW* and concentration of the depletant, the measurements reveal distinct $I(q)$ depending on the wrapping polymer (Figure 4a). PEO750x8- and PEO2000x4-wrapped NCs show pronounced increases in $I(q)$ at low q and a prominent peak around $qa = 2.5$ atop the shoulder of the form factor, while that of the PEO5000x2-wrapped NCs features a broad plateau. This primary peak and additional peaks at higher q are even more apparent in the structure factor, $S(q)$, found by dividing $I(q)$ by the scattering pattern of dilute NCs (Figure S19). The height of the primary peaks in $S(q)$ are 3.68 and 3.79 for PEO750x8- and PEO2000x4-wrapped NCs respectively, exceeding the Hansen criterion value of 2.85 for crystallization.[93] Upon increasing PEO graft *MW*, the primary peak shifts to smaller q, indicating larger NC−NC spacing. The NC spacing trend is consistent with the trends in effective size based on the osmotic second virial coefficient and in hydrodynamic size determined by DLS (Table S1) for particles without depletant. These consistencies imply the polymer shell remains surrounding individual nanocrystals in the assemblies, which facilitates the observed ease of reversibility from aggregates to discrete, stabilized NCs (Figure 2b and Video S1).

Employing Beaucage's unified function to fit the SAXS intensity, the structure on different length scales within each assembled sample may be defined and further analyzed.[94−96] Besides the form factor level, present even for the PEO5000x2-wrapped NCs that resist assembly, for the PEO750x8- and PEO2000x4-wrapped cases there is an additional "assembly" level from which we can extract a radius of gyration and Porod exponent (Table S5 and Figure S20). The radius of gyration for the *assemblies* reveals aggregates of NCs 700−800 nm in radius. The Porod exponent P is 3.7 for both, which indicates how the intensity scales with q for the region and is typically used to define an assembly fractal dimension. This fits the scattering intensity at low q to a power law (where $I(q) \propto q^{-P}$ or $P = 6 - D_s$) to extract a surface fractal dimension (D_s) of 2.3. A surface fractal dimension of 2 indicates a smooth or more densely packed surface while 3 indicates a rough surface (and a crossover with mass fractal dimension of 3).[35,97−99]

https://doi.org/10.1021/acs.jpcc.2c06279
J. Phys. Chem. C 2022, 126, 19507−19518

Thus, the NCs are tightly packed, tending toward crystallization, with their spacing controlled by the polymer shell into clusters of hundreds of thousands of NCs each.

The assembly behaviors observed for the different wrapping polymers can be rationalized by PMF obtained from the coarse-grained MD simulations (Figure 4b). Polymer graft *MW* and grafting density were varied while maintaining a depletant *MW* of 20 kDa. Similar to the arguments presented in Figure 3, the experimentally observed aggregation for the systems with PEO750x8- and PEO2000x4-wrapped NCs is consistent with their corresponding PMF having deep attractive wells. Likewise, the stability of PEO5000x2-wrapped NCs against aggregation make sense given the purely repulsive nature of its corresponding PMF. Furthermore, the minimum in the computed PMF occurs at larger NC separation distance for PEO2000x4 wrapping than for PEO750x8 wrapping, consistent with the experimental trend in NC spacing inferred from SAXS analysis.

Among the copolymers experimentally studied, the effective PEO graft *MW* and graft density were simultaneously varied, but it would be informative to independently assess the impact of each on depletion interactions. While it was infeasible to probe all combinations experimentally, we used MD simulations to sweep the corresponding parameter space and calculate the resulting PMF. For a fixed depletant *MW* of 20 kDa, we calculated the PMF for different combinations of graft length and graft density, determining in each case whether the interactions remain purely repulsive or otherwise assessing the depth of the attractive PMF well formed (Figure 4c). Purely repulsive interactions were observed irrespective of the *MW* of the polymer graft for the systems with the lowest graft density (corresponding to the lowest graft density experimentally probed). While for higher graft densities, NC attractions develop and strengthen with increasing graft density or increasing graft *MW*. Combinations of higher graft density and graft *MW*s are not accessible using simulations due to the high number density of monomers in the region between the NCs. However, on the basis of the trends presented in Figure 4c, we expect strong attractive interactions between NCs in this regime.

The influence of the wrapping polymer characteristics on the strength of depletion attraction can be rationalized based on the interplay between the two competing forces, namely, the steric repulsions arising due to the grafted polymer chains and the effective exclusion of the depletants from the region between the NCs. Specifically, as graft *MW* and density increase, the increased steric repulsion is more than compensated by stronger depletion-induced attractions due to the larger grafts' ability to more effectively exclude depletants from the NC overlap volume. This causes a greater osmotic pressure imbalance and a corresponding deepening of the attractive well. Moreover, the presence of a threshold grafting density below which the purely repulsive interactions persist no matter the graft *MW* indicates the importance of maintaining considerable polymer grafting to effectively exclude the depletant polymers from intercalating between grafts in the region between the NCs. The exclusion of depletants from this region is necessary to create sufficient osmotic pressure imbalance and thereby induce effective attraction between the NCs. Of course, in the absence of polymer grafts, depletion leads to attractions, but experimentally some density of polymer grafting is typically necessary to disperse nanoparticles. Overall, phase behavior and spatial arrangement of the NCs depend sensitively on, and thus may be deliberately modified by, the design of the surface copolymer.

Through mediating the NC assembled structure (or lack thereof), polymer wrapping also impacts the resulting mechanical and optical properties. Viscosity measurements of the three polymer-wrapped NC colloids with depletant were made with a shear flow experiment with shear rates from 10^{-2} to 8600 s^{-1}. At the lowest shear rates the PEO5000x2-wrapped NC sample had viscosity below the instrumental detection limits. We observe two distinct regimes (Figure 5): low shear

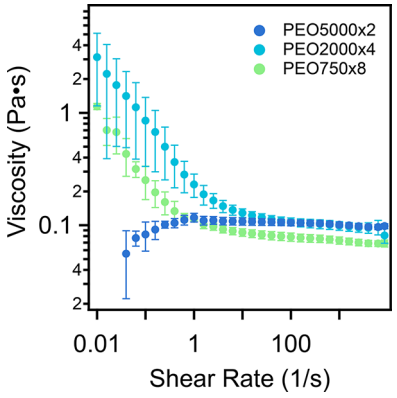

Figure 5. Viscosity as a function of shear rate for each polymer-wrapped NC (ϕ_{NC} = 0.025) with the addition of 35 kDa PEG depletant (250 mg/mL).

rate behavior is influenced by depletion attractions, and high shear rate behavior is dictated by the polymer-wrapped NCs themselves. Both assemblies (PEO750x8- and PEO2000x4-wrapped NCs) exhibit decreases in viscosity as shear rate increases, i.e., they undergo shear thinning, while the stable dispersion (PEO5000x2-wrapped NCs) exhibits modest shear thickening at low shear rates (Figure 5). The shear thickening may be attributed to shear-induced cluster formation.[100] In contrast, the observed shear thinning at very low rates corresponds to the disruption of clusters already present in the assemblies as they are gradually pulled apart by shear.[101,102] Earlier experiments have also noted when attractions are increased beyond the spinodal and through the gel boundary, zero shear rate viscosity diverges and becomes immeasurable instead of plateauing to a finite viscosity at low shear.[103−105] However, this scenario is not consistent with the rheological behavior of our samples, which flow and do not form gels.

The shear thinning behavior can be fit to a power law: $\eta \propto \dot{\gamma}^{-\alpha}$, where η is the viscosity, $\dot{\gamma}$ the shear rate, and α the power exponent. With increasing assembled network strength, α trends toward one.[106] The assemblies have α values of 0.77 ± 0.12 (PEO750x8-wrapped NCs) and 0.58 ± 0.04 (PEO2000x4-wrapped NCs). The apparently "stronger" assembly for the PEO750x8 case suggests stronger depletion attractions, consistent with the MD simulations comparing these two wrapping polymers.

The Peclet number ($Pe = 6\pi a^3\dot{\gamma}\eta/kT$, where a is the cluster size), which compares the importance of flow vs diffusion, equals one at the onset of shear thinning. Though the onset of shear thinning occurs below the experimentally accessible range of shear rates, by inputting the lowest shear rate measured, we may calculate a limiting (minimum) cluster size

https://doi.org/10.1021/acs.jpcc.2c06279
J. Phys. Chem. C 2022, 126, 19507−19518

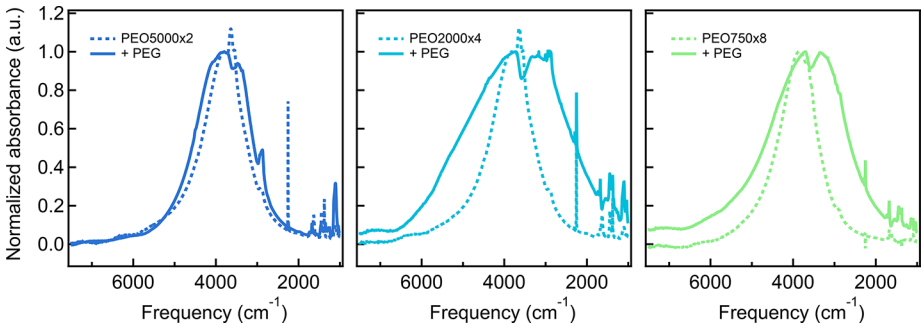

Figure 6. Optical absorption spectra of each polymer-wrapped NC dilute dispersion and concentrated colloid with depletant.

of 700 nm in the depletion-induced assemblies, which is consistent with the USAXS analysis.

At high shear rate, viscosity (η_∞) increases modestly for increasing graft length/decreasing PEO graft density. In general, it may be expected that as the particle volume fraction increases, the viscosity increases. In addition, it has been observed that for nanoparticles with end-grafted polymers in a polymer melt, as particle "softness" increases, which is defined as the ratio of surface polymer shell thickness to the particle core radius, viscosity increases.[107] Because increasing graft length of the surface polymer (PEO_{MW}: 750 → 5000) increases both particle softness and effective volume fraction, the observed higher viscosities are consistent with these trends in related systems.

Finally, to ascertain how characteristics of the wrapping polymer impact optical properties of the NC assemblies, extinction spectra were measured for dilute NC dispersions and for the concentrated colloids with PEG depletant. LSPR peaks are known to broaden when NCs are in close contact due to optical coupling. While the PEO5000x2-wrapped NCs exhibited minimal change in spectral line shape upon addition of depletant, both the PEO2000x4- and PEO750x8-wrapped NCs exhibit substantial peak broadening and red-shifts in the LSPR frequency (Figure 6). (Note that the sharp peaks present in the spectra are due to vibrational modes of the surface polymer (Figure S5) and the depletant polymer.) The spectral changes upon assembly are due to LSPR coupling between neighboring NCs, which are much closer together as compared to NCs in dispersion.[108] Thus, variations in the surface polymer shell dictate NC assembly structure across length scales from nearest neighbors to NC clusters, which in turn tunes both rheological and optical properties due to collective, structure-dependent contributions.

CONCLUSIONS

We showed that polymer-wrapped NCs have excellent stability resulting from polymer-shell-derived repulsions, yet these repulsions can be overcome by adding sufficiently high-*MW* depletants to induce assembly of NC clusters. The balance between repulsion and attraction depends on the architecture of the wrapping polymer, especially the density and *MW* of the polymer grafts, and how effective these grafts are at excluding the nonadsorbing depletant polymer. This interplay results in a depletant *MW* threshold as well as a graft density threshold for assembly. NC interactions varied from purely repulsive to longer-range attractive with increasing depletant *MW*, avoiding altogether the strong, short-range attactions that tend to promote colloidal gelation. Nontrivially, we learned that, regardless of graft length, if the grafting density is too low, depletion-driven assembly will not occur for the conditions explored. Above these thresholds, the attractive well becomes deeper for denser and longer polymer grafts, with enhanced depletion attraction dominating the greater repulsions. These trends deviate from expectations based on isotropic depletion interactions of hard-sphere-like colloids and nonadsorbing polymers, but they mirror phenomena observed in grafted nanoparticle−polymer composites and are a result of the commensurate length scales of the particles, surface polymers, and depletants on the nanoscale. The results offer fresh stimulus to consider how the molecular structure of the coating polymer might be designed for desired interactions and phase behaviors.[109,110] The configurational entropy of mobile grafts on colloids may influence assembly by allowing for rearrangement and structural stabilization.[111] As such, this may prompt the adoption of simulations which consider finite graft mobility to reveal quantitative differences in interactions and guide further experimental exploration. The impact of molecular-level changes specific to nanoscale assembly may translate to similar effects for proteins with complex surface architectures and shapes as well as microparticles with rough surfaces. While depletion is still understood to be in effect, complex particle geometries may lead to deviations from simple models used to predict phase behavior.

The discovered thresholds for assembly may motivate further studies in responsive depletion attractions or fueled assemblies.[112,113] Depletion attractions are a powerful and broadly applicable approach for assembly because they are reversible and do not rely on chemically specific interactions between components. Reversibility was demonstrated here and in previous NC depletion studies by simply diluting the depletant[36] or using thermoresponsive depletants which collapse or swell upon crossing a critical temperature threshold, thus modulating attractions due to the change in depletant size.[39] The modularity of adding an exogenous molecular component to induce attractions provides flexibility in the design of new systems,[30] and there are many opportunities for studying new, reconfigurable depletants within the widely studied field of responsive polymers.[114−117] While the present results establish the phase behavior of polymer-wrapped NCs with depletion attractions, the dynamics of assembly or reconfiguration in response to such perturbations are yet to be investigated. Recent work has used photon correlation imaging paired with dynamic light scattering,[118,119] and X-ray photon correlation spectroscopy[72,120] to investigate structural evolution with time toward assembly as well as the homogeneity (or heterogeneity) of the structures.

https://doi.org/10.1021/acs.jpcc.2c06279
J. Phys. Chem. C 2022, 126, 19507−19518

With the assembly of polymer-wrapped NCs via depletion attractions, we have introduced a model system with many "knobs" that may be tuned to deliberately assemble or disassemble the NCs and modify resulting properties. This materials platform is amenable to (1) employing NC building blocks with different optical, magnetic, or catalytic properties, (2) adding new functionalities to NCs at their surfaces via copolymers to introduce additional, complementary properties in the assemblies, and (3) developing new methods to dynamically tune NC−NC attractions. In addition to changing surface polymer graft length, density, and composition, changes in solvent quality and consequently Flory−Huggins coefficients for the surface polymer as well as the depletant polymer may be used to fine-tune the resulting NC morphology.[121,122] Polymers at the surface of NCs may be designed to mediate new properties in NC assemblies, and the choice of depletion as the source of attractions enables the exchange of these surface polymers independently of the assembly methodology. Importantly, understanding which individual contributions are critical to the formation of the resulting morphology on the nanoscale establishes the foundation to design assemblies with targeted, structure-dependent properties. These insights lay a strong foundation for future studies, leveraging the tunability and synthetically tunable properties of polymers in conjunction with the physical dynamics of nanoscale assembly.

■ ASSOCIATED CONTENT

Supporting Information

The Supporting Information is available free of charge at https://pubs.acs.org/doi/10.1021/acs.jpcc.2c06279.

Experimental procedures and additional characterization data (PDF)

Video S1 (MP4)

■ AUTHOR INFORMATION

Corresponding Authors

Thomas M. Truskett − *McKetta Department of Chemical Engineering, University of Texas at Austin, Austin, Texas 78712, United States; Department of Physics, University of Texas at Austin, Austin, Texas 78712, United States;* orcid.org/0000-0002-6607-6468; Email: truskett@che.utexas.edu

Delia J. Milliron − *McKetta Department of Chemical Engineering, University of Texas at Austin, Austin, Texas 78712, United States;* orcid.org/0000-0002-8737-451X; Email: milliron@che.utexas.edu

Authors

Allison M. Green − *McKetta Department of Chemical Engineering, University of Texas at Austin, Austin, Texas 78712, United States;* orcid.org/0000-0002-7734-4202

Sanket Kadulkar − *McKetta Department of Chemical Engineering, University of Texas at Austin, Austin, Texas 78712, United States;* orcid.org/0000-0002-2834-7677

Zachary M. Sherman − *McKetta Department of Chemical Engineering, University of Texas at Austin, Austin, Texas 78712, United States;* orcid.org/0000-0001-9798-287X

Thomas M. Fitzsimons − *McKetta Department of Chemical Engineering, University of Texas at Austin, Austin, Texas 78712, United States;* orcid.org/0000-0001-7316-475X

Charles K. Ofosu − *Department of Chemistry, University of Texas at Austin, Austin, Texas 78712, United States;* orcid.org/0000-0002-9536-4733

Jiajun Yan − *Materials Sciences Division, Lawrence Berkeley National Laboratory, Berkeley, California 94720, United States;* orcid.org/0000-0003-3286-3268

David Zhao − *McKetta Department of Chemical Engineering, University of Texas at Austin, Austin, Texas 78712, United States; Department of Chemical Engineering, University of California, Santa Barbara, Santa Barbara, California 93106, United States*

Jan Ilavsky − *X-ray Sciences Division, Argonne National Laboratory, Lemont, Illinois 60439, United States*

Adrianne M. Rosales − *McKetta Department of Chemical Engineering, University of Texas at Austin, Austin, Texas 78712, United States;* orcid.org/0000-0003-0207-7661

Brett A. Helms − *The Molecular Foundry, Lawrence Berkeley National Laboratory, Berkeley, California 94720, United States; Materials Sciences Division, Lawrence Berkeley National Laboratory, Berkeley, California 94720, United States;* orcid.org/0000-0003-3925-4174

Venkat Ganesan − *McKetta Department of Chemical Engineering, University of Texas at Austin, Austin, Texas 78712, United States;* orcid.org/0000-0003-3899-5843

Complete contact information is available at: https://pubs.acs.org/10.1021/acs.jpcc.2c06279

Notes

The authors declare no competing financial interest.

■ ACKNOWLEDGMENTS

This work was primarily supported by the National Science Foundation through the Center for Dynamics and Control of Materials: an NSF Materials Research Science and Engineering Center (NSF MRSEC) under Cooperative Agreement DMR-1720595. This work was also supported by the Welch Foundation (F-1848, F-1599, and F-1696). SAXS data were collected at UT Austin with an instrument acquired under NSF MRI Grant CBET-1624659. This research used resources of the Advanced Photon Source, a U.S. Department of Energy (DOE) Office of Science user facility operated for the DOE Office of Science by Argonne National Laboratory under Contract DE-AC02-06CH11357. The authors acknowledge the Texas Advanced Computing Center (TACC) for providing computing resources that have contributed to the research results reported within this paper. Work at the Molecular Foundry—including polymer synthesis and characterization—was supported by the Office of Science, Office of Basic Energy Sciences, of the U.S. Department of Energy under Contract DE-AC02-05CH11231.

■ REFERENCES

(1) Agrawal, A.; Cho, S. H.; Zandi, O.; Ghosh, S.; Johns, R. W.; Milliron, D. J. Localized Surface Plasmon Resonance in Semiconductor Nanocrystals. *Chem. Rev.* **2018**, *118*, 3121−3207.

(2) Talapin, D. V.; Lee, J.-S.; Kovalenko, M. V.; Shevchenko, E. V. Prospects of Colloidal Nanocrystals for Electronic and Optoelectronic Applications. *Chem. Rev.* **2010**, *110*, 389−458.

(3) Kang, J.; Valenzuela, S. A.; Lin, E. Y.; Dominguez, M. N.; Sherman, Z. M.; Truskett, T. M.; Anslyn, E. V.; Milliron, D. J. Colorimetric Quantification of Linking in Thermoreversible Nanocrystal Gel Assemblies. *Sci. Adv.* **2022**, *8*, eabm7364.

(4) Dominguez, M. N.; Howard, M. P.; Maier, J. M.; Valenzuela, S.; Sherman, Z. M.; Reimnitz, L. C.; Kang, J.; Cho, S. H.; Gibbs, S. L.; Menta, A. K.; et al. Assembly of Linked Nanocrystal Colloids by Reversible Covalent Bonds. *Chem. Mater.* **2020**, *32*, 10234−10245.
(5) Sherman, Z. M.; Kim, K.; Kang, J.; Roman, B. J.; Crory, H. S. N.; Conrad, D. L.; Valenzuela, S. A.; Lin, E. Y.; Dominguez, M. N.; Gibbs, S. L.; et al. Plasmonic Response of Complex Nanoparticle Assemblies. *ChemRxiv: Materials Science*, September 15, 2022, DOI: 10.26434/chemrxiv-2022-rkqw8 (accessed 2022-10-13).
(6) Wen, Y. H.; Lu, Y.; Dobosz, K. M.; Archer, L. A. Structure, Ion Transport, and Rheology of Nanoparticle Salts. *Macromolecules* **2014**, *47*, 4479−4492.
(7) Yang, T.; Zheng, J.; Cheng, Q.; Hu, Y.-Y.; Chan, C. K. Composite Polymer Electrolytes with Li7La3Zr2O12 Garnet-Type Nanowires as Ceramic Fillers: Mechanism of Conductivity Enhancement and Role of Doping and Morphology. *ACS Appl. Mater. Interfaces* **2017**, *9*, 21773−21780.
(8) Kadulkar, S.; Milliron, D.; Truskett, T.; Ganesan, V. Transport Mechanisms Underlying Ionic Conductivity in Nanoparticle-Based Single-Ion Electrolytes. *J. Phys. Chem. Lett.* **2020**, *11*, 6970−6975.
(9) Kadulkar, S.; Howard, M. P.; Truskett, T.; Ganesan, V. Prediction and Optimization of Ion Transport Characteristics in Nanoparticle-Based Electrolytes Using Convolutional Neural Networks. *J. Phys. Chem. B* **2021**, *125*, 4838−4849.
(10) Rueb, C. J.; Zukoski, C. F. Viscoelastic Properties of Colloidal Gels. *J. Rheol.* **1997**, *41*, 197−218.
(11) Akcora, P.; Liu, H.; Kumar, S. K.; Moll, J.; Li, Y.; Benicewicz, B. C.; Schadler, L. S.; Acehan, D.; Panagiotopoulos, A. Z.; Pryamitsyn, V.; et al. Anisotropic Self-Assembly of Spherical Polymer-Grafted Nanoparticles. *Nat. Mater.* **2009**, *8*, 354−359.
(12) Del Gado, E.; Fiocco, D.; Foffi, G.; Manley, S.; Trappe, V.; Zaccone, A. *Fluids, Colloids and Soft Materials: An Introduction to Soft Matter Physics*; John Wiley & Sons: 2016.
(13) Kadulkar, S.; Banerjee, D.; Khabaz, F.; Bonnecaze, R. T.; Truskett, T.; Ganesan, V. Influence of Morphology of Colloidal Nanoparticle Gels on Ion Transport and Rheology. *J. Chem. Phys.* **2019**, *150*, 214903.
(14) Matter, F.; Luna, A. L.; Niederberger, M. From Colloidal Dispersions to Aerogels: How to Master Nanoparticle Gelation. *Nano Today* **2020**, *30*, 100827.
(15) Duong, J.; Bailey, M. J.; Pick, T. E.; McBride, P. M.; Rosen, E. L.; Buonsanti, R.; Milliron, D. J.; Helms, B. A. Efficient Polymer Passivation of Ligand-Stripped Nanocrystal Surfaces. *J. Polym. Sci. A* **2012**, *50*, 3719−3727.
(16) Nish, A.; Hwang, J.-Y.; Doig, J.; Nicholas, R. J. Highly Selective Dispersion of Single-Walled Carbon Nanotubes Using Aromatic Polymers. *Nat. Nanotechnol.* **2007**, *2*, 640−646.
(17) Samanta, S. K.; Fritsch, M.; Scherf, U.; Gomulya, W.; Bisri, S. Z.; Loi, M. A. Conjugated Polymer-Assisted Dispersion of Single-Wall Carbon Nanotubes: The Power of Polymer Wrapping. *Acc. Chem. Res.* **2014**, *47*, 2446−2456.
(18) Jayaraman, A. Polymer Grafted Nanoparticles: Effect of Chemical and Physical Heterogeneity in Polymer Grafts on Particle Assembly and Dispersion. *J. Polym. Sci. B: Polym. Phys.* **2013**, *51*, 524−534.
(19) Jadhav, S. A.; Scalarone, D.; Brunella, V.; Ugazio, E.; Sapino, S.; Berlier, G. Thermoresponsive Copolymer-Grafted SBA-15 Porous Silica Particles for Temperature-Triggered Topical Delivery Systems. *Express Polym. Lett.* **2017**, *11*, 96−105.
(20) Gao, J.; Li, J.; Benicewicz, B. C.; Zhao, S.; Hillborg, H.; Schadler, L. S. The Mechanical Properties of Epoxy Composites Filled with Rubbery Copolymer Grafted SiO_2. *Polymer* **2012**, *4*, 187−210.
(21) Jiao, Y.; Chou, T.; Akcora, P. Design of Ion-Containing Polymer-Grafted Nanoparticles for Conductive Membranes. *Macromolecules* **2015**, *48*, 4910−4917.
(22) Gittins, D. I.; Caruso, F. Tailoring the Polyelectrolyte Coating of Metal Nanoparticles. *J. Phys. Chem. B* **2001**, *105*, 6846−6852.
(23) Mendelsberg, R. J.; McBride, P. M.; Duong, J. T.; Bailey, M. J.; Llordes, A.; Milliron, D. J.; Helms, B. A. Dispersible Plasmonic Doped Metal Oxide Nanocrystal Sensors that Optically Track Redox Reactions in Aqueous Media with Single-Electron Sensitivity. *Adv. Opt. Mater.* **2015**, *3*, 1293−1300.
(24) Graham, A. J.; Gibbs, S. L.; Saez Cabezas, C. A.; Wang, Y.; Green, A. M.; Milliron, D. J.; Keitz, B. K. In Situ Optical Quantification of Extracellular Electron Transfer Using Plasmonic Metal Oxide Nanocrystals. *ChemElectroChem* **2022**, *9*, e202101423.
(25) Kim, S. H.; Oh, S.; Chae, S.; Lee, J. W.; Choi, K. H.; Lee, K. E.; Chang, J.; Shi, L.; Choi, J.-Y.; Lee, J. H. Exceptional Mechanical Properties of Phase-Separation-Free Mo3Se3−Chain-Reinforced Hydrogel Prepared by Polymer Wrapping Process. *Nano Lett.* **2019**, *19*, 5717−5724.
(26) Arachchige, I. U.; Brock, S. L. Sol−Gel Methods for the Assembly of Metal Chalcogenide Quantum Dots. *Acc. Chem. Res.* **2007**, *40*, 801−809.
(27) Xiong, H.; van der Lelie, D.; Gang, O. DNA Linker-Mediated Crystallization of Nanocolloids. *J. Am. Chem. Soc.* **2008**, *130*, 2442−2443.
(28) Jones, M. R.; Seeman, N. C.; Mirkin, C. A. Programmable Materials and the Nature of the DNA Bond. *Science* **2015**, *347*, 1260901.
(29) Sayevich, V.; Cai, B.; Benad, A.; Haubold, D.; Sonntag, L.; Gaponik, N.; Lesnyak, V.; Eychmüller, A. 3D Assembly of All-Inorganic Colloidal Nanocrystals into Gels and Aerogels. *Angew. Chem., Int. Ed.* **2016**, *55*, 6334−6338.
(30) Green, A. M.; Ofosu, C. K.; Kang, J.; Anslyn, E. V.; Truskett, T. M.; Milliron, D. J. Assembling Inorganic Nanocrystal Gels. *Nano Lett.* **2022**, *22*, 1457−1466.
(31) Song, J.; Rizvi, M. H.; Lynch, B. B.; Ilavsky, J.; Mankus, D.; Tracy, J. B.; McKinley, G. H.; Holten-Andersen, N. Programmable Anisotropy and Percolation in Supramolecular Patchy Particle Gels. *ACS Nano* **2020**, *14*, 17018−17027.
(32) Lekkerkerker, H. N. W.; Tuinier, R. *Colloids and the Depletion Interaction*; Springer: 2011.
(33) Mutch, K. J.; van Duijneveldt, J. S.; Eastoe, J. Colloid−Polymer Mixtures in the Protein Limit. *Soft Matter* **2007**, *3*, 155−167.
(34) Miyazaki, K.; Schweizer, K.; Thirumalai, D.; Tuinier, R.; Zaccarelli, E. The Asakura−Oosawa theory: Entropic Forces in Physics, Biology, and Soft Matter. *J. Chem. Phys.* **2022**, *156*, 080401.
(35) Poling-Skutvik, R.; Lee, J.; Narayanan, S.; Krishnamoorti, R.; Conrad, J. C. Tunable Assembly of Gold Nanorods in Polymer Solutions To Generate Controlled Nanostructured Materials. *ACS Appl. Nano Mater.* **2018**, *1*, 8770885.
(36) Saez Cabezas, C. A.; Ong, G. K.; Jadrich, R. B.; Lindquist, B. A.; Agrawal, A.; Truskett, T. M.; Milliron, D. J. Gelation of Plasmonic Metal Oxide Nanocrystals by Polymer-Induced Depletion Attractions. *Proc. Natl. Acad. Sci. U. S. A.* **2018**, *115*, 8925−8930.
(37) Saez Cabezas, C. A.; Sherman, Z. M.; Howard, M. P.; Dominguez, M. N.; Cho, S. H.; Ong, G. K.; Green, A. M.; Truskett, T. M.; Milliron, D. J. Universal Gelation of Metal Oxide Nanocrystals via Depletion Attractions. *Nano Lett.* **2020**, *20*, 4007−4013.
(38) Zhao, C.; Yuan, G.; Jia, D.; Han, C. C. Macrogel Induced by Microgel: Bridging and Depletion Mechanisms. *Soft Matter* **2012**, *8*, 7036−7043.
(39) Rossi, L.; Sacanna, S.; Irvine, W. T. M.; Chaikin, P. M.; Pine, D. J.; Philipse, A. P. Cubic Crystals from Cubic Colloids. *Soft Matter* **2011**, *7*, 4139−4142.
(40) Rossi, L.; Soni, V.; Ashton, D. J.; Pine, D. J.; Philipse, A. P.; Chaikin, P. M.; Dijkstra, M.; Sacanna, S.; Irvine, W. T. M. Shape-Sensitive Crystallization in Colloidal Superball Fluids. *Proc. Natl. Acad. Sci. U. S. A* **2015**, *112*, 5286−5290.
(41) Zhang, I.; Royall, C. P.; Faers, M. A.; Bartlett, P. Phase Separation Dynamics in Colloid-Polymer Mixtures: The Effect of Interaction Range. *Soft Matter* **2013**, *9*, 2076.
(42) Lu, P. J.; Zaccarelli, E.; Ciulla, F.; Schofield, A. B.; Sciortino, F.; Weitz, D. A. Gelation of Particles with Short-Range Attraction. *Nature* **2008**, *453*, 499−503.

(43) Bibette, J.; Roux, D.; Nallet, F. Depletion Interactions and Fluid-Solid Equilibrium in Emulsions. *Phys. Rev. Lett.* **1990**, *65*, 2470−2473.
(44) Sacanna, S.; Irvine, W. T. M.; Chaikin, P. M.; Pine, D. J. Lock and Key Colloids. *Nature* **2010**, *464*, 575−578.
(45) Li, W.; Delaney, K. T.; Fredrickson, G. H. Self-consistent field theory study of polymer-mediated colloidal interactions in solution: Depletion Effects and Induced Forces. *J. Chem. Phys.* **2021**, *155*, 154903.
(46) Kamp, M.; Hermes, M.; van Kats, C. M.; Kraft, D. J.; Kegel, M.; Dijkstra, W. K. ad; van Blaaderen, A. Selective Depletion Interactions in Mixtures of Rough and Smooth Silica Spheres. *Langmuir* **2016**, *32*, 1233−1240.
(47) Anzini, P.; Parola, A. How Roughness Affects the Depletion Mechanism. *Soft Matter* **2017**, *13*, 5150.
(48) Faers, M.; Luckham, P. Effect of the Steric Stabilizing Layer on the Phase Behavior and Rheology of Small Polystyrene Latex Dispersions Induced by Changes to the Concentration of Non-adsorbing Hydroxyethylcellulose. *Langmuir* **1997**, *13*, 2922−2931.
(49) Ramakrishnan, S.; Fuchs, M.; Schweizer, K. S.; Zukoski, C. F. Concentration Fluctuations in a Model Colloid-Polymer Suspension: Experimental Tests of Depletion Theories. *Langmuir* **2002**, *18*, 1082−1090.
(50) Shah, S. A.; Chen, Y.-L.; Ramakrishnan, S.; Zukoski, C. F. Microstructure of Dense Colloid-Polymer Suspensions and Gels. *J. Phys.: Condens. Matter* **2003**, *15*, 4751−4778.
(51) Ramakrishnan, S.; Fuchs, M.; Schweizer, K. S.; Zukoski, C. F. Entropy Driven Phase Transitions in Colloid−Polymer Suspensions: Tests of Depletion Theories. *J. Chem. Phys.* **2002**, *116*, 2201.
(52) Ramakrishnan, S.; Gopalakrishnan, V.; Zukoski, C. F. Clustering and Mechanics in Dense Depletion and Thermal Gels. *Langmuir* **2005**, *21*, 9917−9925.
(53) Milling, A.; Vincent, B.; Emmett, S.; Jones, A. Depletion Flocculation in Dispersions of Sterically-Stabilised Silica Particles 3. The Effect of Grafted Chain Coverage. *Colloids Surf.* **1991**, *57*, 185−195.
(54) Rosenbaum, D. F.; Zukoski, C. F. Protein Interactions and Crystallization. *J. Cryst. Growth* **1996**, *169*, 752−758.
(55) Finet, S.; Tardieu, A. α-Crystallin Interaction Forces Studied by Small Angle X-ray Scattering and Numerical Simulations. *J. Cryst. Growth* **2001**, *232*, 40−49.
(56) Tanaka, S.; Ataka, M. Protein Crystallization Induced by Polyethylene Glycol: A Model Study Using Apoferritin. *J. Chem. Phys.* **2002**, *117*, 3504−3510.
(57) Vivares, D.; Belloni, L.; Tardieu, A.; Bonnete, F. Catching the PEG-induced Attractive Interaction Between Proteins. *Eur. Phys. J. E* **2002**, *9*, 15−25.
(58) Kulkarni, A.; Zukoski, C. Depletion Interactions and Protein Crystallization. *J. Cryst. Growth* **2001**, *232*, 156−164.
(59) Julius, K.; Weine, J.; Gao, M.; Latarius, J.; Elbers, M.; Paulus, M.; Tolan, M.; Winter, R. Impact of macromolecular Crowding and Compression on Protein−Protein Interactions and Liquid−Liquid Phase Separation Phenomena. *Macromolecules* **2019**, *52*, 1772−1784.
(60) Cheng, R.; Li, J.; Rios de Anda, I.; Taylor, T. W. C.; Faers, M. A.; Anderson, J. L. R.; Seddon, A. M.; Royall, C. P. Protein−Polymer Mixtures in the Colloid Limit: Aggregation, Sedimentation, and Crystallization. *J. Chem. Phys.* **2021**, *155*, 114901.
(61) Speer, S. L.; Stewart, C. J.; Sapir, L.; Harries, D.; Pielak, G. J. Macromolecular Crowding Is More than Hard-Core Repulsions. *Annu. Rev. Biophys.* **2022**, *51*, 267−300.
(62) Clarke, J.; Cavanna, F.; Crowell, A. D.; Melcher, L.; Houser, J. R.; Graham, K.; Green, A. M.; Stachowiak, J. C.; Truskett, T. M.; Milliron, D. J.; et al. Depletion-Driven Morphological Control of Bundled Actin Networks. *arXiv: Soft Condensed Matter*, October 1, 2022, arXiv:2205.01864 (accessed 2022-10-13).
(63) Chatterjee, A. P.; Schweizer, K. S. Microscopic Theory of Polymer-Mediated Interactions between Spherical Particles. *J. Chem. Phys.* **1998**, *109*, 10464−10476.
(64) Fuchs, M.; Schweizer, K. S. Structure of Colloid-Polymer suspensions. *J. Phys.: Condens. Matter* **2002**, *14*, R239.
(65) Bolhuis, P. G.; Meijer, E. J.; Louis, A. A. Colloid-Polymer Mixtures in the Protein Limit. *Phys. Rev. Lett.* **2003**, *90*, 068304.
(66) Ganesan, V.; Ellison, C. J.; Pryamitsyn, V. Mean-Field Models of Structure and Dispersion of Polymer-Nanoparticle Mixtures. *Soft Matter* **2010**, *6*, 4010−4025.
(67) Fleer, G. J.; Tuinier, R. Analytical Phase Diagrams for Colloids and Non-Adsorbing Polymer. *Adv. Colloid Interface Sci.* **2008**, *143*, 1−47.
(68) Ganesan, V.; Jayaraman, A. Theory and Simulation Studies of Effective Interactions, Phase Behavior and Morphology in Polymer Nanocomposites. *Soft Matter* **2014**, *10*, 13−38.
(69) Sherman, Z. M.; Green, A. M.; Howard, M. P.; Anslyn, E. V.; Truskett, T. M.; Milliron, D. J. Colloidal Nanocrystal Gels from Thermodynamic Principles. *Acc. Chem. Res.* **2021**, *54*, 798−807.
(70) Calvin, J. J.; Brewer, A. S.; Alivisatos, A. P. The Role of Organic Ligand Shell Structures in Colloidal Nanocrystal Synthesis. *Nat. Synth.* **2022**, *1*, 127−137.
(71) Kumar, S. K.; Jouault, N.; Benicewicz, B.; Neely, T. Nanocomposites with Polymer Grafted Nanoparticles. *Macromolecules* **2013**, *46*, 3199−3214.
(72) Srivastava, S.; Kishore, S.; Narayanan, S.; Sandy, A. R.; Bhatia, S. R. Multiple Dynamic Regimes in Colloid-Polymer Dispersions: New Insight Using X-Ray Photon Correlation Spectroscopy. *J. Polym. Sci. B Polym. Phys.* **2016**, *54*, 752−760.
(73) Jansons, A. W.; Hutchison, J. E. Continuous Growth of Metal Oxide Nanocrystals: Enhanced Control of Nanocrystal Size and Radial Dopant Distribution. *ACS Nano* **2016**, *10*, 6942−6951.
(74) Dong, A.; Ye, X.; Chen, J.; Kang, Y.; Gordon, T.; Kikkawa, J.; Murray, C. A Generalized Ligand-Exchange Strategy Enabling Sequential Surface Functionalization of Colloidal Nanocrystals. *J. Am. Chem. Soc.* **2011**, *133*, 998−1006.
(75) Bailey, M. J.; van der Weegen, R.; Klemm, P. J.; Baker, S. L.; Helms, B. A. Stealth Rare Earth Oxide Nanodiscs for Magnetic Resonance Imaging. *Adv. Healthcare Mater.* **2012**, *1*, 437−442.
(76) Maho, A.; Saez Cabezas, C. A.; Meyertons, K. A.; Reimnitz, L. C.; Sahu, S.; Helms, B. A.; Milliron, D. J. Aqueous Processing and Spray Deposition of Polymer-Wrapped Ti-Doped Indium Oxide Nanocrystals as Electrochromic Thin Films. *Chem. Mater.* **2020**, *32*, 8401−8411.
(77) Ilavsky, J.; Zhang, F.; Andrews, R. N.; Kuzmenko, I.; Jemian, P. R.; Levine, L. E.; Allen, A. J. Development of Combined Microstructure and Structure Characterization Facility for In Situ and Operando Studies at the Advanced Photon Source. *J. Appl. Crystallogr.* **2018**, *51*, 867−882.
(78) Meng, D.; Kumar, S. K.; Lane, J. M. D.; Grest, G. S. Effective Interactions Between Grafted Nanoparticles in a Polymer Matrix. *Soft Matter* **2012**, *8*, 5002−5010.
(79) Lee, H.; Venable, R. M.; Mackerell, A. D., Jr.; Pastor, R. W. Molecular Dynamics Studies of Polyethylene Oxide and Polyethylene Glycol: Hydrodynamic Radius and Shape Anisotropy. *Biophys. J.* **2008**, *95*, 1590−1599.
(80) Garcia, A. G.; Tuinier, R. Tuning the Phase Diagram of Colloid-Polymer Mixtures via Yukawa Interactions. *Phys. Rev. E* **2016**, *94*, 062607.
(81) De Roo, J.; Yazdani, N.; Drijvers, E.; Lauria, A.; Maes, J.; Owen, J. S.; van Driessche, I.; Niederberger, M.; Wood, V.; Martins, J. C.; et al. Probing SolventLigand Interactions in Colloidal Nanocrystals by the NMR Line Broadening. *Chem. Mater.* **2018**, *30*, 5485−5492.
(82) van Rijssel, J.; Peters, V. F. D.; Meeldijk, J. D.; Kortschot, R. J.; van Dijk-moes, R. J. A.; Petukhov, A. V.; Erné, B. H.; Philipse, A. P. Size-Dependent Second Virial Coefficients of Quantum Dots from Quantitative Cryogenic Electron Microscopy. *J. Phys. Chem. B* **2014**, *118*, 11000−11005.
(83) Ofosu, C. K.; Truskett, T. M.; Milliron, D. J. Solvent-Ligand Interactions Govern Stabilizing Repulsions Between Colloidal Metal Oxide Nanocrystals. *ChemRxiv: Nanoscience*, August 25, 2022, DOI: 10.26434/chemrxiv-2022-0hx82 (accessed 2022-10-13).

(84) Izor, S.; Schantz, A.; Jawaid, A.; Grabowski, C.; Dagher, T.; Koerner, H.; Park, K.; Vaia, R. Coexistence and Phase Behavior of Solvent-Polystyrene-Grafted Gold Nanoparticle Systems. *Macromolecules* **2021**, *54*, 10435−10446.
(85) Schroer, M. A.; Lehmkuhler, F.; Möller, J.; Lange, H.; Grubel, G.; Schulz, F. Pressure-Stimulated Supercrystal Formation in Nanoparticle Suspensions. *J. Phys. Chem. Lett.* **2018**, *9*, 4720−4724.
(86) Devanand, K.; Selser, J. C. Asymptotic Behavior and Long-Range Interactions in Aqueous Solutions of Poly(ethy1ene oxide). *Macromolecules* **1991**, *24*, 5943−5947.
(87) Harton, S. E.; Kumar, S. K. Mean-field Theoretical Analysis of Brush-Coated Nanoparticle Dispersion in Polymer Matrices. *J. Polym. Sci. B: Polym. Phys.* **2008**, *46*, 351−358.
(88) Trombly, D. M.; Ganesan, V. Curvature Effects upon Interactions of Polymer-Grafted Nanoparticles in Chemically Identical Polymer Matrices. *J. Chem. Phys.* **2010**, *133*, 154904.
(89) Srivastava, S.; Agarwal, P.; Archer, L. A. Tethered Nanoparticle−Polymer Composites: Phase Stability and Curvature. *Langmuir* **2012**, *28*, 6276−6281.
(90) Striolo, A. Colloidal Brushes in Complex Solutions: Existence of a Weak Midrange Attraction due to Excluded-Volume Effects. *Phys. Rev. E* **2006**, *74*, 041401.
(91) Striolo, A.; Egorov, S. Steric Stabilization of Spherical Colloidal Particles: Implicit and Explicit Solvent. *J. Chem. Phys.* **2007**, *126*, 014902.
(92) Fortini, A.; Dijkstra, M.; Tuinier, R. Phase Behaviour of Charged Colloidal Sphere Dispersions with Added Polymer Chains. *J. Phys.: Condens. Matter* **2005**, *17*, 7783−7803.
(93) Hansen, J. P.; Verlet, L. Phase Transitions of the Lennard-Jones System. *Phys. Rev.* **1969**, *184*, 151.
(94) Beaucage, G. Approximations Leading to a Unified Exponential/Power-Law Approach to Small-Angle Scattering. *J. Appl. Crystallogr.* **1995**, *28*, 717−728.
(95) Beaucage, G.; Kammler, H. K.; Pratsinis, S. E. Particle Size Distributions from Small-Angle Scattering using Global Scattering Functions. *J. Appl. Crystallogry.* **2004**, *37*, 523−535.
(96) Beaucage, G. Combined Small-Angle Scattering for Characterization of Hierarchically Structured Polymer Systems over Nano-to-Micron Meter. *Polymer Science: a Comprehensive Reference (Elsevier)* **2012**, 399−409.
(97) Besselink, R.; Stawski, T. M.; van Driessche, A. E. S.; Benning, L. G. Not Just Fractal Surfaces, but Surface Fractal Aggregates: Derivation of the Expression for the Structure Factor and its Applications. *J. Chem. Phys.* **2016**, *145*, 211908.
(98) Hurd, A. J.; Schaefer, D. W.; Martin, J. E. Surface and Mass Fractals in Vapor-Phase Aggregates. *Phys. Rev. A* **1987**, *35*, 2361−2364.
(99) Schaefer, D. W.; Keefer, K. D. Structure of Random Porous Materials: Silica Aerogels. *Phys. Rev. Lett.* **1986**, *56*, 2199−2202.
(100) Osuji, C. O.; Kim, C.; Weitz, D. A. Shear Thickening and Scaling of the Elastic Modulus in a Fractal Colloidal System with Attractive Interactions. *Phys. Rev. E* **2008**, *77*, 0620402.
(101) Dharmaraj, V. L.; Godfrin, P. D.; Liu, Y.; Hudson, S. D. Rheology of Clustering Protein Solutions. *Biomicrofluidics* **2016**, *10*, 043509.
(102) Berli, C. L. A.; Quemada, D.; Parker, A. Modelling the Viscosity of Depletion Flocculated Emulsions. *Colloids Surf., A* **2002**, *203*, 11−20.
(103) Gopalakrishnan, V.; Zukoski, C. F. Effect of Attractions on Shear Thickening in Dense Suspensions. *J. Rheol.* **2004**, *48*, 1321.
(104) Gopalakrishnan, V.; Shah, S. A.; Zukoski, C. F. Cage Melting and Viscosity Reduction in Dense Equilibrium Suspensions. *J. Rheol.* **2005**, *49*, 383.
(105) Winter, H. H. Glass Transition as the Rheological Inverse of Gelation. *Macromolecules* **2013**, *46*, 2425−2432.
(106) Kobelev, V.; Schweizer, K. S. Dynamic Yielding, Shear Thinning, and Stress Rheology of Polymer-Particle Suspensions and Gels. *J. Chem. Phys.* **2005**, *123*, 164903.
(107) McEwan, M.; Green, D. Rheological Impacts of Particle Softness on Wetted Polymer-Grafted Silica Nanoparticles in Polymer Melts. *Soft Matter* **2009**, *5*, 1705−1716.
(108) Agrawal, A.; Singh, A.; Yazdi, S.; Singh, A.; Ong, G. K.; Bustillo, K.; Johns, R. W.; Ringe, E.; Milliron, D. J. Resonant Coupling between Molecular Vibrations and Localized Surface Plasmon Resonance of Faceted Metal Oxide Nanocrystals. *Nano Lett.* **2017**, *17*, 2611−2620.
(109) Martin, T. B.; Dodd, P. M.; Jayaraman, A. Polydispersity for Tuning the Potential of Mean Force between Polymer Grafted Nanoparticles in a Polymer Matrix. *Phys. Rev. Lett.* **2013**, *110*, 018301.
(110) Feng, H.; Bohmer, M.; Fokkink, R.; Sprakel, J.; Leermakers, F. Reentrant Stabilization of Grafted Nanoparticles in Polymer Solutions. *J. Phys. Chem. B* **2015**, *119*, 12938−12946.
(111) Hu, H.; Ruiz, P. S.; Ni, R. Entropy Stabilizes Floppy Crystals of Mobile DNA-Coated Colloids. *Phys. Rev. Lett.* **2018**, *120*, 048003.
(112) Rao, A.; Roy, S.; Pillai, P. P. Temporal Changes in Interparticle Interactions Drive the Formation of Transiently Stable Nanoparticle Precipitates. *Langmuir* **2021**, *37*, 1843−1849.
(113) van Ravensteijn, B. G. P.; Voets, I. K.; Kegel, W. K.; Eelkema, R. Out-of-Equilibrium Colloidal Assembly Driven by Chemical Reaction Networks. *Langmuir* **2020**, *36*, 10639−10656.
(114) Zhang, Q.; Weber, C.; Schubert, U. S.; Hoogenboom, R. Thermoresponsive Polymers with Lower Critical Solution Temperature: From Fundamental Aspects and Measuring Techniques to Recommended Turbidimetry Conditions. *Mater. Horiz.* **2017**, *4*, 109.
(115) Bertrand, O.; Gohy, J. Photo-Responsive Polymers: Synthesis and Applications. *Polym. Chem.* **2017**, *8*, 52.
(116) Wei, M.; Gao, Y.; Li, X.; Serpe, M. J. Stimuli-Responsive Polymers and Their Applications. *Polym. Chem.* **2017**, *8*, 127.
(117) Sun, X.; Chwatko, M.; Lee, H.; Bachman, J. L.; Reuther, J. F.; Lynd, N. A.; Anslyn, E. V. Chemically Triggered Synthesis, Remodeling, and Degradation of Soft Materials. *J. Am. Chem. Soc.* **2020**, *142*, 3913−3922.
(118) Lattuada, E.; Caprara, D.; Piazza, R.; Sciortino, F. Spatially Uniform Dynamics in Equilibrium Colloidal Gels. *Sci. Adv.* **2021**, *7*, eabk2360.
(119) Duri, A.; Sessoms, D. A.; Trappe, V.; Cipelletti, L. Resolving Long-Range Spatial Correlations in Jammed Colloidal Systems Using Photon Correlation Imaging. *Phys. Rev. Lett.* **2009**, *102*, 085702.
(120) Jhalaria, M.; Jimenez, A. M.; Mathur, R.; Tekell, M. C.; Huang, Y.; Narayanan, S.; Benicewicz, B. C.; Kumar, S. K. Long-Term Aging in Miscible Polymer Nanocomposites. *Macromolecules* **2022**, *55*, 4502−4515.
(121) Domènech, B.; Plunkett, A.; Kampferbeck, M.; Blankenburg, m.; Bor, B.; Giuntini, D.; Krekeler, T.; Wagstaffe, M.; Noei, H.; Stierle, A.; et al. Modulating the Mechanical Properties of Supercrystalline Nanocomposite Materials via Solvent-Ligand Interactions. *Langmuir* **2019**, *35*, 13893−13903.
(122) Haddadi, S.; Skepo, M.; Forsman, J. From Attraction to Repulsion to Attraction: Non-monotonic Temperature Dependence of Polymer-Mediated Interactions in Colloidal Dispersions. *ACS Nanosci. Au* **2021**, *1*, 69−80.

https://doi.org/10.1021/acs.jpcc.2c06279
J. Phys. Chem. C 2022, 126, 19507−19518